Structural and dynamical studies of hybrid siloxane–silica materials

B. Lebeau,[a] J. Maquet,[a] C. Sanchez,*[a] F. Beaume[b] and F. Lauprêtre[b]

[a]*Laboratoire de Chimie de la Matière Condensée, Université P. et M. Curie, URA CNRS 1466, 4 place Jussieu, 75252 Paris cedex 05, France*

[b]*Laboratoire de Physico-Chimie Structurale et Macromoléculaire, Ecole Supérieure de Physique et de Chimie Industrielles de la Ville de Paris, URA CNRS 278, 10 rue Vauquelin, 75231 Paris cedex 05, France*

Hybrid siloxane–silica coatings have been prepared by hydrolysis and condensation of *N*-[3-triethoxysilylpropyl]-2,4-dinitrophenylamine (TSDP) and tetramethoxysilane (TMOS) precursors. Hetero- and homo-condensations between both precursors have been demonstrated to occur in the early stages of the process *via* ^{17}O and ^{29}Si nuclear magnetic resonance (NMR) in solution. These hybrids can be described as nanocomposites made of polysiloxane-based domains cross-linked by silica-based nanoparticles, as evidenced by solid-state NMR, differential scanning calorimetry (DSC) and Fourier-transform infrared (FTIR) studies. Moreover, the high degree of interpenetration occurring in these materials is evidenced by the presence of some Q and T subunits sequestered within these polysiloxane and silica-based domains, respectively. The high-resolution solid-state ^{13}C NMR technique has shown that the mobility of the propyl 2,4-dinitrophenylamine chromophores is correlated with the glass-transition phenomenon of the matrix.

The mild synthetic conditions of the sol–gel process allow the introduction of 'fragile' organic molecules inside inorganic networks,[1–3] leading to so-called hybrid organic–inorganic materials.[4–9] The properties of hybrid materials depend not only on the chemical nature of the organic and inorganic components but also on the interface between the phases. The general tendency is to increase interfacial interactions by creating an intimate mixing between organic and inorganic networks.[9] Moreover, the formation of chemical bonds between organic and inorganic species should minimize phase separation and, thus, led to formation of nano- or even molecular composites. These new hybrid organic–inorganic materials offer a wide range of interesting properties especially in the field of optics (solid-state dye lasers, sensors, photochromic and non-linear optical devices, *etc.*).[10–13]

Quadratic non-linear optical properties of organic–inorganic hybrids containing optically active dipolar chromophores are usually observed after an electrical field poling process.[14–17] This process induces the orientation of the organic dyes and cancels the centrosymmetry inherent to amorphous sol–gel matrices. However, because of thermal relaxation processes, organic dyes tend to loose their induced orientation with time and the second harmonic generated signal decreases. Consequently, the optical properties of these materials are strongly dependent on the nature of the bonding between the organic dye and the matrix, and on the characteristics of the matrix. Up to know, the best results have been obtained with siloxane–oxide matrices prepared from monofunctional alkoxysilanes $R'Si(OR)_3$ or multifunctional alkoxysilanes $\{R'[Si(OR)_3]_2$, $R'[Si(OR)_3]_3\}$ co-reacted with metal alkoxides such as $Si(OR)_4$.[18–23] The organic group R′ contains the non-linear optical (NLO) chromophore bound to the network by a covalent Si—C bond, stable towards hydrolysis.

We have previously reported the synthesis and NLO properties of hybrid siloxane–oxide compounds made from hydrolysis and condensation of TSDP (T units) and TMOS (Q units) precursors.[19] Depending on the chemical composition, the second hamonic generation (SHG) values ranged between 2.5 and 10 pm V^{-1}. Preliminary NMR and DSC characterizations have shown that such systems made of siloxane polymers cross-linked with silica species exhibit a glass-transition temperature T_g which increases with the TMOS content. In this first approach, the relaxation behaviour of the NLO chromophore was correlated with the glass-transition phenomenon of the matrix.

This paper describes a more complete structural and dynamical characterization of these hybrid siloxane–silica systems made by hydrolysis and condensation of TSDP and TMOS.

The first stages of polymerization were followed by liquid-state ^{29}Si NMR spectroscopy which is a very convenient technique to study these systems.[24,25]

The condensation reactions were investigated by ^{17}O NMR of sols which allows one to follow homocondensation (formation of T–O–T and Q–O–Q bridges) and heterocondensation (formation of T–O–Q bridges) reactions between silicon alkoxides.[26] The low natural abundance of the ^{17}O nucleus (3.7×10^{-2}%) and its quadrupole moment renders its detectability difficult. However, the use of ^{17}O enriched water for the hydrolysis of precursors leads to a specific labelling of Si—O*H and Si—O*—Si groups and thus greatly enhances their detectability.

Structural investigations in xerogels were performed by using solid-state ^{29}Si NMR with magic angle spinning (MAS) and FTIR spectroscopy. High-resolution solid-state ^{29}Si NMR using magic angle spinning (MAS), cross-polarization (CP) and proton dipolar decoupling (DD), and DSC experiments were performed to get a better insight of the size and organization of the siloxane (T units) and silica (Q units) species present in these hybrid systems. High-resolution solid-state ^{13}C NMR spectroscopy was used to investigate the mobility of the chromophore *vs.* temperature in these hybrid TSDP/TMOS systems. Among the number of NMR parameters that are sensitive to molecular motions, the variation of the ^{13}C–^{1}H dipolar coupling strength with temperature was chosen to follow the local motions of the chromophores. The strength of the ^{13}C–^{1}H dipolar coupling was determined by the $t_{1/2}$ contact time technique.[27]

Experimental

Synthesis of hybrid siloxane–silica coatings

TSDP was used as the siloxane network precursor bearing the NLO chromophore while TMOS was used as a cross-linking reagent to increase the network rigidity.

Sol–gel coatings with different TSDP : TMOS molar ratios were prepared by using the previously described[19] procedure.

The precursors, TSDP and TMOS, were mixed in acetone and co-hydrolysed with acidic water (HCl; pH = 1) with an H_2O/Si molar ratio of 2. Then, the solution was stirred for 30 min and the resulting sols were aged for 4 h. From these sols, hydrophobic transparent films several micrometres thick were obtained free of cracks and faults. Coatings were prepared by deposition on ordinary soda-lime glass sheets which were previously cleaned and dried. An appropriate amount of solution was poured on the glass sheet and allowed to gel and dry at room temperature. After drying, coatings were ground and cured at 150 °C for 12 h.

In this paper, coatings are labelled T_x/Q_y, where T and Q stand for TSDP and TMOS, respectively and x and y are the molar percentages ($x+y=100$) of the different precursors. T^m ($m=0-3$) and Q^n ($n=0-4$) notations have their well known usual meaning.[28] T and Q refer to the oxo trifunctional $R'-SiO_3$ and tetrafunctional SiO_4 central units, respectively, and m and n are the numbers of Si—O*—Si bridging oxygens attached to the central unit. The notation T^m_i is used for hydrolysed T^m units in solution where i refers to the number of OH groups.

Chemical characterization

NMR experiments. ^{29}Si and ^{17}O NMR spectra of T_x/Q_y hydrolysed solutions were recorded on a MSL 400 Bruker spectrometer working at 79 and 54 MHz, respectively. Samples were put in an 8 mm tube which was in turn placed in a 10 mm tube containing C_6D_6 as lock solvent.

For ^{29}Si NMR experiments, typical spectra were obtained using 160 scans with a pulse width of 5 μs (*ca.* 30 °) and a recycle delay of 10 s. Tetramethylsilane (TMS) was used as a reference for chemical shifts.

For ^{17}O NMR experiment, a 10 μs (90 °) pulse width was used; 1000 scans were accumulated with a 200 ms recycle delay, consistent with the short relaxation times of ^{17}O nuclei.[29] Water was used as a reference for the chemical shifts.

For the ^{17}O NMR experiments TSDP and TMOS were hydrolysed in acetonitrile with acidic ^{17}O-enriched water ($H_2O/Si=0.5$; pH = 1). ^{17}O-enriched water was purchased from ISOTEC (France). Reported ^{17}O NMR data for T—O—T (δ 55–65) bridges, T—OH groups (δ 30), Q—O—Q bridges (δ 20–30), Q—OH groups (δ 10–15) and T—O—Q bridges (δ 45) obtained from hydrolysis of $CH_3Si(OC_2H_5)_3$–$Si(OC_2H_5)_4$ indicate that, at high hydrolysis ratio, the resolution of the ^{17}O NMR spectra is poor.[26] In order to get a better resolution, a low hydrolysis ratio was chosen to prevent extensive condensation reactions and favour the formation of small polymeric species. Acetonitrile was chosen as solvent to avoid ^{17}O exchange between water and solvent. As shown by ^{17}O NMR, the exchange process that occurs between acetone and water (cetol formation) does not occur with acetonitrile within the timescale of the NMR experiments.

High-resolution solid-state ^{29}Si NMR experiments using magic angle spinning (MAS), cross-polarization (CP) and proton dipolar decoupling (DD) were conducted on a MSL 300 Bruker spectrometer. The resonance frequency was 59.7 MHz. The solid samples were spun at 5 kHz in 7 mm diameter ZrO_2 rotors. TMS was used as a reference for chemical shifts.

Solid-state ^{29}Si NMR experiments were conducted with quadrature detection and a radio-frequency (rf) coil which was double-tuned for both ^{29}Si and ^1H. MAS CP DD ^{29}Si NMR spectra were obtained in single-contact experiments by using variable contact times between 1 and 50 ms, and a recycle delay of 10 s. 360 scans were accumulated for each spectrum. The matched spin-lock cross-polarization transfers were carried out with ^{29}Si and ^1H magnetic field strengths of 42 kHz. For high-resolution solid-state ^{29}Si NMR experiments using only magic angle spinning, pulse width and relaxation delays were 2 μs (*ca.* 30 °) and 60 s, respectively. 480 scans were recorded for each spectrum, which corresponds to an 8 h experiment. However, data thus obtained are only semi-quantitative because of the long relaxation time of the silicon nuclei.

High-resolution solid-state ^{13}C NMR experiments using magic angle spinning, cross-polarization proton and dipolar decoupling were conducted at 75 MHz with a Bruker ASX 300 spectrometer, with quadrature detection and an rf coil, which was double-tuned for ^{13}C and ^1H. Experiments were performed on magic angle spinning samples contained in 4 mm diameter ZrO_2 rotors. The spinning speed was of the order of 4 kHz. The matched spin-lock cross-polarization transfers were carried out with ^{13}C and ^1H magnetic field strengths of 62 kHz. $t_{1/2}$ values were obtained from the dependence of the intensities $M(t)$ of the CH_2 carbon lines in cross-polarization experiments as a function of the contact time t. At all temperatures, the whole curve $M(t)=f(t)$ was determined, including a precise evaluation of the maximum magnetization M_{max}, that can be gained from cross-polarization.

^{29}Si NMR spectra were simulated with the WINFIT program[30] to estimate the integrated area for each T^m and Q^n species which correspond to their relative amounts. The mean degree of condensation C was calculated for every T or Q set of components by taking $C(T)=\Sigma_m mt^m/3$ and $C(Q)=\Sigma_n nq^n/4$, where t^m and q^n are the relative amounts measured from simulated NMR spectra for T^m and Q^n species, respectively.

DSC experiments. Differential scanning calorimetry (DSC) experiments were performed on a Perkin-Elmer 7 series instrument, using *ca.* 15 mg of xerogel. The experiments were performed under cycling conditions. First, the temperature was increased from −20 to 145 °C to wipe the sample memory. Then, the starting temperature was set to −20 °C. Heating and cooling rates for each run were fixed to 10 °C min^{-1}. The data were collected during the third run and analysed with the Perkin-Elmer thermal analysis software. The glass-transition temperatures measured by DSC correspond to the midpoint of the heat flow change. For each measurement, an integration area as large as 40 °C was used. The accuracy of the T_g values is ±2 °C depending on the ability to adjust the tangent lines of the curve step.

FTIR experiments. A Nicolet Magna-IR 550 spectrophotometer was used to run Fourier-transform IR experiments. Hybrid T_x/Q_y coatings were ground with KBr and pressed into pellets to record FTIR spectra. 32 scans were accumulated with a resolution of 4 cm^{-1} for each spectrum.

Results and Discussion

^{29}Si and ^{17}O NMR of T_x/Q_y hydrolysed solutions

^{29}Si NMR spectra of T_{100}/Q_0 and T_{50}/Q_{50} hydrolysed solutions obtained at 1 and 4 h after water addition are plotted in Fig. 1. Assignments were made according to data from the literature.[31,32] By comparison with the ^{29}Si NMR studies of the hydrolysis of the methyltriethoxysilane precursor under the same conditions, chemical shifts of species issued from hydrolysis of TSDP are shifted by 2 ppm to higher fields. The spectrum of T_{100}/Q_0 sol aged for 1 h shows three peaks at δ −49, −50.9 and −53 due to T^1 units (T^1_0, T^1_1 and T^1_2, respectively), two peaks at δ −58.5 and −60.5 due to linear T^2 units (T^2_0 and T^2_1, respectively), two peaks at δ −49.6 and −57 due to cyclic T^2 units (trimer and tetramer cyclic T^2 units, respectively) and a resonance at δ −55 which is probably due to constrained cyclic T^3 units.[33,34] At 4 h after water addition, the intensities

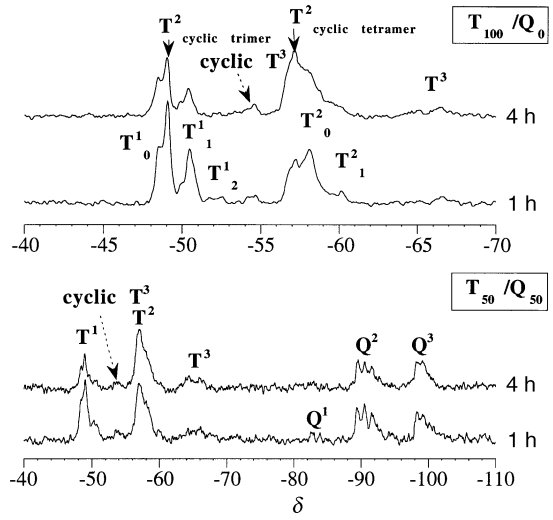

Fig. 1 Liquid-state ^{29}Si NMR spectra of T_{100}/Q_0 and T_{50}/Q_{50} hydrolysed solutions at 1 h and 4 h after water addition

of T^2 units peaks are higher while the intensities of T^1 units peaks are smaller. A new resonance is observed at δ −65/67 which can be assigned to T^3 units. The spectrum of the hydrolysed T_{50}/Q_{50} solution aged for 1 h shows weak resonances around δ −65/−67 due to T^3 units whose intensity increases strongly upon 4 h ageing of the sol. Weak NMR resonances around δ −84 assigned to Q^1 units are only observed on the spectrum recorded at 1 h after water addition. In both spectra, recorded at 1 and 4 h after water addition, resonances assigned to Q^2 and Q^3 units are observed around δ −92 and −100, respectively. The resonances of Q^1 units are observed in both T_0/Q_{100} sol spectra recorded at 1 h and 4 h after water addition.

The relative amounts of T^m and Q^n species determined from spectrum simulation and the degrees of condensation of T and Q units are reported in Table 1. They indicate a better completion of condensation reactions upon ageing.

The degree of completion of condensation reactions for both T and Q units is higher in the T_{50}/Q_{50} hydrolysed solution than in T_{100}/Q_0 and T_0/Q_{100} hydrolysed solutions. This phenomenon can be likely related to heterocondensation reactions occurring between some T and Q units (*vide infra*).

Both T_{100}/Q_0 and T_{50}/Q_{50} spectra exhibit ^{29}Si resonances assigned to T cyclic arrangements. From spectral simulations, the relative amount of T cyclic species was estimated to be equal to 42 and 54% at 4 h after water addition in T_{100}/Q_0 and T_{50}/Q_{50} hydrolysed solutions, respectively. The highest value observed in the T_{50}/Q_{50} hydrolysed solution can be related to a better completion of condensation reactions of T units when the hydrolysis is performed in the presence of Q units.

Fig. 2 shows ^{17}O NMR spectra of hydrolysed solutions of TSDP, TMOS and a mixture of both in a 1:1 molar ratio, recorded at 4 h after water addition. Minor resonances around δ −26, −9 and 6 are due to oxygen nuclei of residual

Table 1 Relative amounts and degrees of condensation C of T^m and Q^n units in T_{100}/Q_0, T_{50}/Q_{50} and T_0/Q_{100} hydrolysed solutions, at 1 and 4 h after water addition

T_x/Q_y	t/h	T^1	T^2	T^3	C(T)	Q^1	Q^2	Q^3	C(Q)
T_{100}/Q_0	1	35	65	0	55	—	—	—	—
T_{100}/Q_0	4	17	74	9	64	—	—	—	—
T_{50}/Q_{50}	1	7	86	7	67	2	57	41	60
T_{50}/Q_{50}	4	5	76	20	72	0	46	54	64
T_0/Q_{100}	1	—	—	—	—	7	53	40	58
T_0/Q_{100}	4	—	—	—	—	6	45	49	61

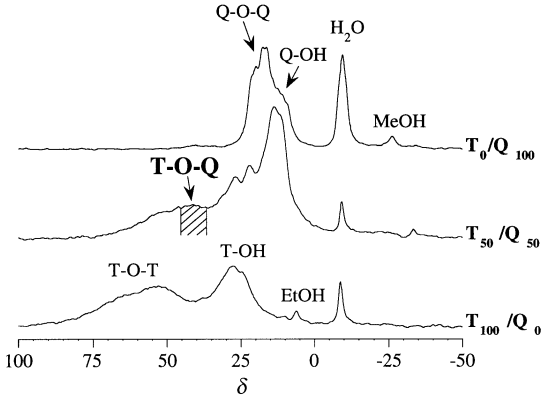

Fig. 2 Liquid-state ^{17}O NMR spectra of T_0/Q_{100}, T_{50}/Q_{50} and T_{100}/Q_0 hydrolysed solutions at 4 h after water addition

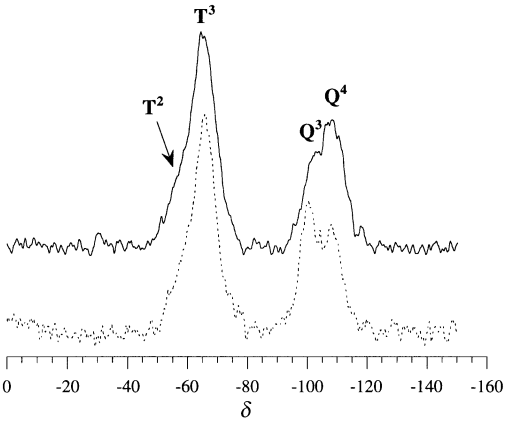

Fig. 3 High-resolution ^{29}Si MAS NMR spectra of the uncured (– – –) and cured (—) T_{60}/Q_{40} hybrid coatings

methanol, water and ethanol, respectively. The spectrum of the hydrolysed TMOS solution shows resonances around δ 13 and 20 due to Q—OH groups and Q—O—Q bridges, respectively.[26] The behaviour of the hydrolysed TSDP solution is different.

Resonances around δ 30 are due to T—OH groups and large resonances around δ 55 and 65 are due to T—O—T bridges. The spectrum of the TSDP–TMOS hydrolysed solution exhibits resonances characteristic of Q—OH, T—OH groups and Q—O—Q, T—O—T bridges and a new broad resonance around δ 42 which was assigned to T—O—Q bridges.[26] The resonance of T—O—Q bridges is observed with a lower intensity on the spectrum of the TSDP–TMOS hydrolysed solution recorded at 10 min after water addition. This observation indicates that heterocondensation of some T and Q units occurs in the early stages of condensation reactions. The amount of T—O—Q bridges increases with time. This is in agreement with the high stability of the siloxane–silica bridges.[26]

Solid-state ^{29}Si MAS NMR

As an example, ^{29}Si MAS NMR spectra of air-dried and thermally cured T_{60}/Q_{40} coatings are shown in Fig. 3. The degrees of condensation, C, for T and Q units measured from the concentration of each species *vs.* TMOS content are reported in Table 2.

The degrees of condensation of T and Q units are higher in the xerogels than in the sols. This difference demonstrates that a large number of condensation and cross-linking reactions still occur upon solvent removal. The uncured T_x/Q_y systems exhibit degrees of condensation C(T) and C(Q) which increase with TMOS content. This phenomenon is related to the mutual

Table 2 Relative amounts and degrees of condensation C of T and Q units in uncured and cured T_x/Q_y xerogels obtained from ^{29}Si MAS NMR data (relative errors in values reported are 2%)

sample	uncured		cured	
T_x/Q_y	C(T)	C(Q)	C(T)	C(Q)
T_{100}/Q_0	85	—	89	—
T_{80}/Q_{20}	89	83	96	92
T_{60}/Q_{40}	95	88	95	94
T_{40}/Q_{60}	92	87	97	93

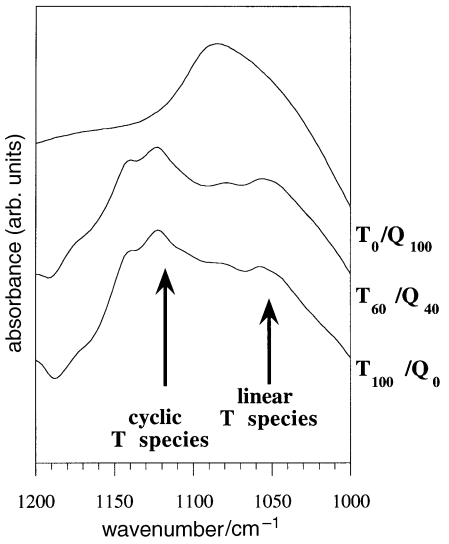

Fig. 4 FTIR spectra of the T_0/Q_{100}, T_{60}/Q_{40} and T_{100}/Q_0 hybrid coatings in the antisymmetric Si—O—Si stretching region

dependence of the hydrolysis–condensation rates of T units by Q units.

After thermal curing, as the result of an enhancement of cross-linking reactions, the degrees of condensation for both T and Q units are much higher, which corroborates the fact that these systems act as thermosets.

FTIR

As indicated in a previous section, ^{29}Si NMR experiments in solution have shown that T units form linear and cyclic arrangements. However, ^{29}Si MAS NMR does not provide sufficient resolution to differentiate linear and cyclic species in the xerogels. The following FTIR experiments were carried out to investigate the distribution of linear and cyclic species in TSDP/TMOS xerogels. Fig. 4 displays the FTIR spectra of T_x/Q_y xerogels in the antisymmetric Si—O—Si stretching region between 1200 and 1000 cm^{-1}. The FTIR spectrum of the T_0/Q_{100} xerogel exhibits a strong band at 1090 cm^{-1} with a shoulder at 1180 cm^{-1} due to the transversal and longitudinal modes of the antisymmetric Si—O—Si stretching, respectively.[35] The antisymmetric Si—O—Si stretching vibration band observed in the FTIR spectra of xerogels containing T units exhibits several components which reveal the presence of species with different structures and symmetries. According to Deng *et al.*,[36] the antisymmetric Si—O—Si stretching can be separated into two main components. The vibration band located at higher energy (1120 cm^{-1}) is usually assigned to T polycyclic caged structures while the band located at lower energy (1050 cm^{-1}) is due to T linear structures.[36,37] Whatever the xerogel composition, the band located at 1120 cm^{-1} is more intense than the band at 1050 cm^{-1}. This result shows that cyclic and linear T species observed in sols are both present in the solid state. Moreover, the relative amount of T cyclic species seems more important than the amount of T linear species.

As evidenced by ^{29}Si MAS NMR, these hybrid networks are made of $(T—T)_a$ units heterocondensed with $(Q—Q)_b$ species. They can be described as composites made of silica domains linked to siloxane polymers.[8] Siloxane (T—O—T) and silica (Q—O—Q) based species linked through stable T—O—Q bridges are formed during the first stages of the process. Because the heterocondensation occurs in the early stages it should limit phase separation between siloxane and silica species.The degree of interpenetration between $(T—T)_a$ and $(Q—Q)_b$ segments is an important parameter on which segmental mobility and, consequently, the relaxation of the chromophores which are grafted inside such hybrid networks, depend.[38] DSC experiments and NMR relaxation measurements described below were carried out in order to investigate this.

DSC experiments

The glass-transition temperatures (T_g) measured by DSC for uncured and cured T_x/Q_y samples are reported in Fig. 5. Only one T_g is observed in the temperature range from 20 to 100 °C.

For both uncured and cured samples, T_g is shifted to higher values with increasing amounts of TMOS. For a given composition, T_g values increase upon curing. This behaviour can be related to the increase in the degree of condensation and cross-linking of the polymers which lead to restricted segmental mobility in T_x/Q_y hybrid systems.

Increase of T_g in T_x/Q_y xerogels with the TMOS content implies that these hybrids are not an immiscible two-phase system.[39] If TSDP/TMOS systems were miscible blends, then extrapolation of data reported in Fig. 5 by using the Gordon–Taylor or Fox expressions[40,41] would lead to a T_g value for the T_0/Q_{100} xerogel of the order of 160 °C which is in strong disagreement with the T_g of silica estimated around 1200 °C[42] and the T_g of silica containing 20 ppm of residual OH groups estimated at around 950 °C.[43] From these data the T_g of silica xerogel containing a large amount of hydroxy groups could be estimated as between 500 and 900 °C.[43] Therefore, TSDP/TMOS xerogels are two-phase partially miscible blends[39] and the T_g measured by DSC refers only to the polysiloxane network (*i.e.* the network made from T units).

The variations of the heat capacity ΔC_p (per gram of polysiloxane) at T_g is plotted *vs.* the TMOS mass content in Fig. 6 (full line). If all the T units were participating in the glass transition, whatever the TMOS content, the corrected ΔC_p should be the same (dashed line in Fig. 6). However, the corrected ΔC_p decreases with TMOS content, indicating that the amount of T units which do not participate in the glass

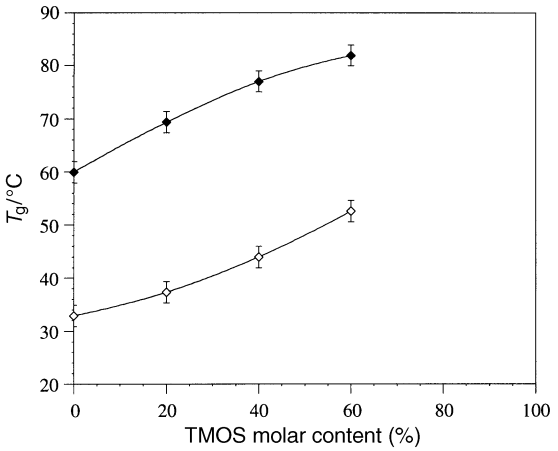

Fig. 5 T_g values *vs.* TMOS molar content in T_x/Q_y hybrid coatings (◇, uncured; ◆, cured)

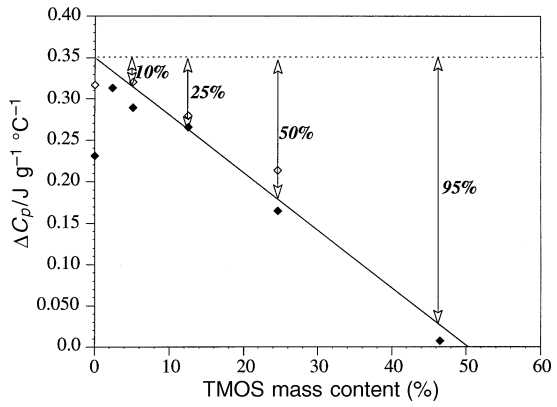

Fig. 6 Variation of the heat capacity ΔC_p at T_g in T_x/Q_y hybrid coatings *vs.* TMOS mass content. The full line fit shows the average behaviour or the ΔC_p *vs.* TMOS mass content. Open and filled diamonds refer to different samples.

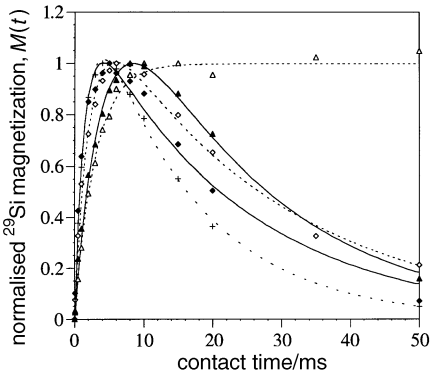

Fig. 7 Variation of the ^{29}Si magnetization of T^3 (+), Q^3 (◆, ◇) and Q^4 (▲, △) units in T_{60}/Q_{40} (+, ◆, ▲) and T_0/Q_{100} (◇, △) xerogels as a function of contact time

transition increases with the TMOS content. The relative amount of T units which do not participate in the polysiloxane glass transition has been estimated from the difference between the theoretical and experimental ΔC_p curves (dashed and full lines, respectively) and is reported in Fig. 6. The number of T units that participate in the polysiloxane glass transition for T_x/Q_y systems containing more than 50% by mass of TMOS is very low. T units that do not participate in glass transition are probably too constrained. They probably belong to smaller $(T-T)_a$ segments trapped in silica domains.

Dynamics of polarization transfer in ^{29}Si NMR experiments

The dynamics of magnetization transfer during cross-polarization is governed by the proton bath. It is sensitive to the number of protons, the silicon–proton and proton–proton distances and the proton mobility.[44] This technique allows one to investigate the homogeneity of a sample.[45]

Fig. 7 shows the intensity of the ^{29}Si magnetization for T^3, Q^3 and Q^4 units in T_{60}/Q_{40} and T_0/Q_{100} xerogels as a function of the cross-polarization contact time under the Hartmann–Hahn condition in a single-contact experiment.[46] The initial rise and the later decline of the ^{29}Si magnetization observed for each plot are due to the cross-polarization by the closest protons, spin diffusion and the manifestation of the relaxation of the spin-locked ^{1}H magnetization.[44]

For the xerogels containing siloxane units, all T units have similar dynamics of magnetization transfer. In this case, the magnetization transfer is mainly provided by the protons of the 2,4-dinitrophenylaminopropyl group which are at relatively small distances from the ^{29}Si nuclei of interest.

For the T_0/Q_{100} xerogel, the initial rise on the left side observed for Q^3 and Q^4 units is slower than the initial rise of the T units. Such a difference is due to the longer ^{29}Si–^{1}H distance of neighbouring protons which are responsible for the magnetization transfer. For Q^3 units, the magnetization transfer is provided by protons in hydroxy or residual methoxy groups attached to silicon nuclei, while for Q^4 units, magnetization transfer is provided by more distant protons, typically from hydroxy or residual methoxy groups of Q^3 or Q^2 linked to Q^4 silicon nuclei. The different distances of neighbouring protons for Q^3 and Q^4 are also responsible for the faster decay observed at long contact times for the Q^3 units as compared with the Q^4 units.

In the T_{60}/Q_{40} xerogel, the dynamics of magnetization transfer of Q^3 and Q^4 at short contact times shows an intermediate behaviour between the behaviour of Q^3 and Q^4 units of T_0/Q_{100} and T units, respectively. These results indicate that the proton baths surrounding Q^3 and Q^4 units in the T_{60}/Q_{40} and the T_0/Q_{100} xerogels are different. This difference can be related to the presence of T units close to Q units in the T_{60}/Q_{40} xerogel. It is usually reported that magnetization transfer in cross-polarization experiments probes distances of the order of one nanometre. Consequently, in the binary T_x/Q_y systems, Q units observed by MAS CP DD ^{29}Si NMR are in the close proximity of T units.

The ^{29}Si–^{1}H cross-polarization technique restricts detection to silicon nuclei that are near protons. For the T_{60}/Q_{40} xerogel, the comparison between the relative amounts of Q units determined from MAS and MAS CP DD (with a 5 ms contact time) ^{29}Si NMR spectra shows that *ca.* 55% of the Q^4 units are observed by MAS CP DD ^{29}Si NMR. In the conclusion derived from the DSC and solid-state ^{29}Si NMR experiments reported above, this result shows a high degree of interpenetration for T and Q units in the T_{60}/Q_{40} xerogel.

MAS CP DD ^{13}C NMR

For a given T_x/Q_y composition the T_g measured by DSC and the temperature of depolarization (the temperature for which the non-linear optical response decreases) measured by the SHG experiment are in good agreement.[19] They are related to the dynamical behaviour of the chromophores but do not provide specific information on the local mobility in xerogels.

MAS CP DD ^{13}C NMR experiments were carried out to investigate the mobility of the CH_2 groups of the propyl chain (*i.e.* chromophore spacer) (see Fig. 8).

For very short contact times, the carbon and its n strongly coupled protons can be considered as an isolated CH_n system. The strength of the ^{13}C–^{1}H dipolar coupling of such a system can be estimated by measuring the contact time $t_{1/2}$ necessary to obtain half of the maximum polarization M_{max}. Assuming that the C—H bond length is 1.09 Å, calculated $t_{1/2}$ values for a rigid lattice are around 24 and 17 μs for CH and CH_2 groups, respectively. Experimental $t_{1/2}$ values longer than these rigid-lattice values are evidence for a reduction of the ^{13}C–^{1}H dipolar coupling by motional processes whose frequencies are higher than 10^5 Hz.[27]

The MAS CP DD ^{13}C NMR spectra and line assignments of T_{100}/Q_0 xerogel recorded at room temperature with contact times of 1 ms and 20 μs are shown in Fig. 8. The intensity of the ^{13}C magnetization *vs.* contact time for the $CH_2(1)$ carbon in the T_{100}/Q_0 xerogel at different temperatures is shown in Fig. 9. The $t_{1/2}$ values measured from the curves $M(t)=f(t)$ at different temperatures for the three CH_2 carbons of the chromophore spacer in the T_{100}/Q_0 xerogel are reported in Table 3. At room temperature and 60 °C, the three CH_2 carbons have short $t_{1/2}$ values corresponding to a nearby rigid-lattice behaviour which indicates that these carbons do not undergo any molecular motion in the $t_{1/2}$ frequency domain between 25 and 60 °C. At 70 °C, the $CH_2(3)$ carbon which is adjacent to the

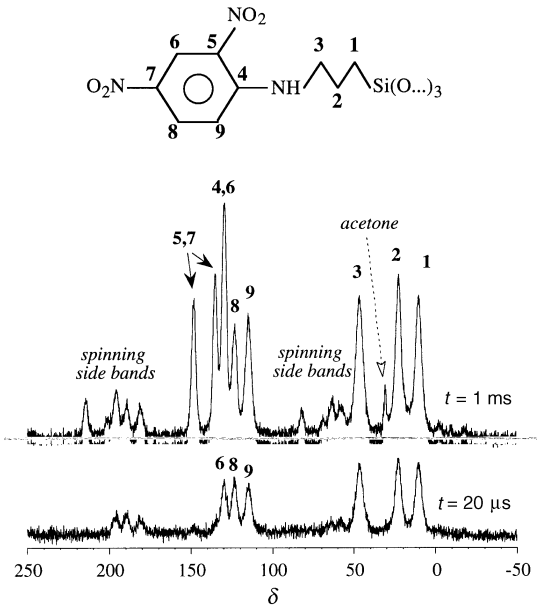

Fig. 8 High-resolution ^{13}C MAS CP DD NMR spectra of the T_{100}/Q_0 xerogel recorded with 20 µs and 1 ms contact times

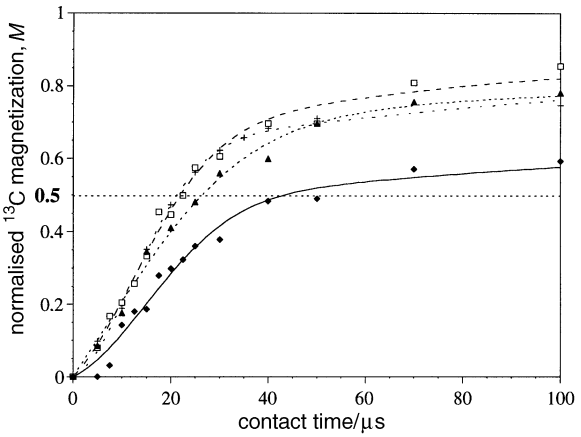

Fig. 9 ^{13}C NMR magnetization variations of $CH_2(1)$ carbon as a function of contact time in T_{100}/Q_0 xerogel at 25 (+), 60 (□), 70 (▲) and 80 °C (▲)

Table 3 $t_{1/2}$ Values measured for $CH_2(1)$, $CH_2(2)$ and $CH_2(3)$ carbons in T_{100}/Q_0 xerogels at different temperatures (accuracy in reported values is 1s)

CH_2	25 °C	60 °C	70 °C	80 °C
1	21	21	26	42
2	22	22	26	40
3	20	21	19	30

2,4-dinitrophenylamino group has $t_{1/2}=19$ µs, characteristic of a rigid-lattice behaviour. On the other hand, $CH_2(1)$ and $CH_2(2)$ carbons have longer $t_{1/2}$ values of 26 µs which indicate the existence of molecular motions involving the ^{13}C–^{1}H internuclear vector. At 80 °C the three CH_2 carbons have $t_{1/2}$ longer than rigid-lattice $t_{1/2}$ values. We have also measured the $t_{1/2}$ value for the CH(9) carbon as a function of temperature in order to investigate the mobility of the phenyl group. At 25 and 60 °C, the CH(9) carbon in the T_{100}/Q_0 xerogel has a $t_{1/2}=22$ µs characteristic of a rigid-lattice CH $t_{1/2}$ value. Above 60 °C peaks due to aromatic carbons become broader and overlap which renders it impossible to measure CH(9) carbon $t_{1/2}$ values. A significant decrease of the signal to noise ratio

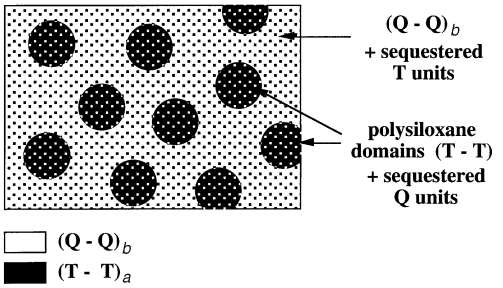

Fig. 10 Schematic of the microstructure of the hybrid TSDP/TMOS coatings

was also observed at 70 °C. The decrease of the signal to noise ratio and line broadening indicate motion of aromatic carbons.

It should be noted that there is a difference of 30 °C between the glass-transition temperature (33 ± 2 °C) measured by DSC and the temperature (>60 °C) for which the amplitude of local motions as observed by NMR begins to increase for $CH_2(1)$ and $CH_2(2)$ carbons. This difference is due to the fact that $t_{1/2}$ values are sensitive to relatively high frequency modes (>10^5 Hz) while DSC is sensitive to lower frequency modes (*ca.* 1 Hz). By taking into account the temperature shift between T_g measured by DSC and T_g observed by NMR in the $t_{1/2}$ frequency domain, one is led to the conclusion that, for the T_{100}/Q_0 xerogel, the increase in the amplitude and/or frequency of $CH_2(1)$ and $CH_2(2)$ carbons motions at T_g+30 °C can be assigned to the increase in mobility associated with the glass-transition phenomenon of the polysiloxane network. The amplitude and/or frequency of $CH_2(1)$ and $CH_2(2)$ carbons motions increase at somewhat lower temperatures because these CH_2 carbons are closest to the polysiloxane main chain. The fact that the amplitude and/or frequency of $CH_2(3)$ carbon motions start to increase above 70 °C indicates that chromophores are constrained in the matrix.

Conclusion

The present work deals with the structural and dynamical investigation of hybrid siloxane–silica coatings constructed by hydrolysis and condensation from TSDP and TMOS precursors. These hybrid materials were reported to have second-order NLO properties.[19]

FTIR, ^{17}O and ^{29}Si NMR experiments pointed out the existence of linear and cyclic siloxane $(T-T)_a$ oligomers and silica $(Q-Q)_b$ units linked through stable T—O—Q bridges formed in the early stages of the process.

The degrees of condensation of T and Q units are higher in xerogels than in the sols and this difference demonstrates that a large amount of condensation and cross-linking reactions still occur upon solvent removal.

The glass-transition phenomenon observed by DSC in these hybrid materials corresponds to the glass transition of the polysiloxane network. The glass-transition temperature increases with the TMOS content while the apparent variation of heat capacity at T_g decreases. These results, as well as the analysis of the polarization transfer in MAS CP DD ^{29}Si NMR experiments, are consistent with the relatively high degree of interpenetration of T and Q units. Therefore, these hybrid TSDP/TMOS coatings can be described as nanocomposites made of silica-rich domains and siloxane-rich domains. Many Q and T species are mutually sequestered at the nanometre scale. Their microstructure is schematically pictured in Fig. 10. The white part corresponds to the silica-rich phase inside which some T units (black dots) are sequestered. The black spheres correspond to the polysiloxane-rich phase which participates in the glass-transition phenomenon and contains Q units (white dots). The size of the polysiloxane and silica

domains depends not only on the chemical composition but also on the drying procedure and consequently on the solvent and sample thickness. Results reported in this paper were obtained on 50–100 μm thick coatings whereas NLO optical characterizations are usually performed on 1–3 μm thick films. Future structural investigations should also be performed on thin coatings.

The mobility of the NLO chromophores, as observed by high-resolution solid-state ^{13}C NMR, is correlated with the glass-transition phenomenon of the matrix. Dielectric relaxation experiments in a large frequency range are in progress in order to improve the understanding of the relationships between the structure and the dynamical behaviour of NLO chromophores in these hybrid systems.

The authors would like to thank Roland Hierle for the DSC measurements. DRET and CNRS are also acknowledged for the financial support.

References

1 D. Avnir, D. Levy and R. Reisfeld, *J. Phys. Chem*., 1984, **88**, 5956.
2 H. Schmidt and B. Seiferling, *Mater. Res. Soc. Symp. Proc*., 1986, **73**, 10.
3 R. Reisfeld, in *Sol–gel Opt. SPIE Proc*., ed. J. D. Mackenzie and D. R. Ulrich, Washington, DC, 1990, vol. 1328, p.29.
4 H. Schmidt, A. Kaiser, H. Patzelt and H. Sholze, *J. Phys*., 1982, **12**, C9.
5 H. Schmidt, H. Scholze and A. Kaiser, *J. Non-Cryst. Solids*, 1984, **63**, 1.
6 G. L. Wilkes, B. Orler and H.H. Huang, *Polym. Prepr*., 1985, **26**, 300.
7 G. -S. Sur and J.E. Mark, *Eur. Polym. J*. 1985, **21**, 1051.
8 C. Sanchez and F. Ribot, *New J. Chem*., 1994, **18**, 1007.
9 B. Novak, *Adv. Mater*., 1993, **5**, 839.
10 *Sol–Gel Opt. I SPIE Proc*., ed. J. D. Mackenzie and D. R. Ulrich, Washington, DC, 1990, vol. 1328.
11 *Sol–Gel Opt. II SPIE Proc*., ed. J. D. Mackenzie, Washington, DC, 1992, vol. 1758.
12 *Sol–Gel Opt. III SPIE Proc*., ed. J. D. Mackenzie, Washington, DC, 1994, vol. 2288.
13 *Sol–Gel Opt., Processing Appl*., ed. L. C. Klein, Kluwer Academic, Boston, 1993.
14 G. Pucetti, I. Ledoux, J. Zyss, P. Griesmar and C. Sanchez, *Polym. Prepr*., 1991, **32**, 61.
15 J. Zyss, G. Pucetti, I. Ledoux, P. Griesmar, J. Livage and C. Sanchez, *Pat*. 1152, March 1991.
16 E. Toussaere, J. Zyss, P. Griesmar and C. Sanchez, *Non Linear Opt*., 1991, **1**, 349; C. Sanchez, P. Griesmar, E. Toussaere, G. Puccetti, I. Ledoux and J. Zyss., *Non-linear Opt*., 1992, **4**, 245.
17 P. Griesmar, C. Sanchez, G. Pucetti, I. Ledoux and J. Zyss, *Mol. Eng*., 1991, **1**, 205.
18 J. Kim, J. L. Plawsky, R. LaPeruta and G. M. Korenowski, *Chem. Mater*., 1992, **4**, 249; J. Kim, J. L. Plawsky, E. Van Wagenen and G. M. Korenowski, *Chem. Mater*., 1993, **5**, 1118.
19 B. Lebeau, J. Maquet, C. Sanchez, E. Toussaere, R. Hierle and J. Zyss, J. Mater. Chem., 1994, **4**, 1855.
20 Z. Yang, C. Xu, B. Wu, L. R. Dalton, S. Kalluri, W. H. Steier, Y. Shi and J. H. Bechtel, *Chem. Mater*., 1994, 6, 1899.
21 H.W. Oviatt, K.J. Shea, S. Kalluri, Y. Shi, W. Steier and L.R. Dalton, *Chem. Mater*., 1995, **7**, 493.
22 D. Reihl, F. Chaput, Y. Levy, J.-P. Boilot, F. Kajzar and P.A. Chollet, *Chem. Phys. Lett*., 1995, **245**, 36.
23 B. Lebeau, C. Sanchez, S. Brasselet, J. Zyss, G. Froc and M. Dumont, *New J. Chem*., 1996, **20**, 13; B. Lebeau, C. Sanchez, S. Brasselet and J. Zyss, in *Better Ceramics Through Chemistry VII : Organic/Inorganic Hybrid Materials*, *Mater. Res. Soc. Symp. Proc*., ed. B. K. Coltrain, C. Sanchez, D. W. Schaefer and G. L. Wilkes, Pittsburgh, 1996, vol. 435, p.395.
24 F. Babonneau, in *Better Ceramics Through Chemistry VI*, *Mater. Res. Soc. Symp. Proc*., ed. A. K. Cheetham, C. J. Brinker, M. L. Mecartney and C. Sanchez, Pittsburgh, 1995, vol. 346, p.949; F. Babonneau, V. Gualandris and M. Pauthe, in *Better Ceramics Through Chemistry VII : Organic/Inorganic Hybrid Materials*, *Mater. Res. Soc. Symp. Proc*., ed. B. K. Coltrain, C. Sanchez, D. W. Schaefer, G. L. Wilkes, Pittsburgh, 1996, vol. 435, p.119.
25 T. M. Alam, R. A. Assink and D. L. Loy, *Chem. Mater*., 1996, **8**, 2366.
26 F. Babonneau, J. Maquet and J. Livage, *Chem. Mater*., 1995, **7**, 1050; F. Babonneau, J. Maquet and J. Livage, *J. Sol–Gel Sci. Technol., Ceramics Trans*., 1995, **55**, 53.
27 F. Lauprêtre, L. Monnerie and J. Virlet, *Macromolecules*, 1984, **17**, 397; F. Lauprêtre, *NMR Basic Princ. Prog*., 1994, **30**, 63.
28 R. H. Glaser, G. L. Wilkes and C. E. Bronnimann, *J. Non-Cryst. Solids*, 1989, **113**, 73.
29 A. R. Bassindale and K. H. Pannell, *J. Chem. Soc., Perkin Trans. 2*, 1990, 1801.
30 D. Massiot, H. Thiele and A. Germanus, *Bruker Rep*., 1994, **140**, 43.
31 F. Brunet, unpublished results.
32 Y. Sugahara, S. Okada, S. Sato, K. Kuroda and C. Kato, *J. Non-Cryst. Solids*, 1994, **167**, 21.
33 Engelhardt and D. Michel, in *High-Resolution Solid-State NMR of Silicates and Zeolites*, J. Wiley & Sons, New York, 1987, p.125.
34 L.J. Feher, D.A. Newman and J.F. Walzer, *J. Am. Chem. Soc*., 1989, **11**, 1741.
35 C. C. Perry and X. Li, *Eurogel'91 Symp. Proc*., Saarbrücken, Elsevier, Amsterdam, 1992.
36 Q. Deng, K. A. Mauritz and R. B. Moore, in *Hybrid Organic–Inorganic Composites*, in *ACS Symp. Ser.* 585, ed. E. Mark, C. Y-C Lee and P. A. Bianconi, American Chemical Society, Washington, DC, 1995, p.66.
37 J. F., Brown Jr., L. H., Jr. Vogt and P. I. Prescott, *J. Am. Chem. Soc*., 1964, **86**, 1120; J. F. Brown Jr., *J. Am. Chem. Soc*., 1965, **87**, 4317.
38 Y. Nosaka, N. Tohriiwa, T Kobayashi and N. Fujii, *Chem. Mater*., 1993, **5**, 930.
39 *Comprehensive Polymer Encyclopedia*, vol. 3, p.760.
40 M. Gordon and G. S. Kongorov, *Rubber Chem. Technol*., 1963, **36**, 668.
41 M. Gordon and J. S. Taylor, *J. Appl. Chem*., 1952, **2**, 493.
42 C. Mazières, in *Les Solides Non Cristalline*, Le chimiste, PUF, 1978, 461.
43 M. Prassas and J. Phalippou, personal communication.
44 S. R. Hartmann and E. L. Hahn, *Phys. Rev*., 1962, **128**, 2042; M. Merhing, in *Principles of High Resolution NMR in Solids*, Springer-Verlag, Berlin, Heidelberg, New York, 2nd edn., 1983.
45 R.A. Komoroski, in *High Resolution NMR Spectroscopy of Synthetic Polymers in Bulk, Methods in Stereochemical Analysis no. 7,* ed. P. Marchand, VCH, FL, 1986.
46 A. Pines, M. G. Gibby and J. S. Waugh, *J. Chem. Phys*., 1972, **56**, 1776; 1973, **59**, 519.

Paper 6/07874E; *Received* 20*th November*, 1996